JOURNAL OF MATERIALS SCIENCE **34** (1999) 2217–2227

Investigations on thermally forced hydrolysis and phase formation in aqueous iron(III) nitrate solutions

M. SCHULTZ
Pelikan Produktions AG, Leestr. 1, CH-8132 Egg, Switzerland
E-mail: schulma@phiag.com

W. BURCKHARDT
Hermsdorf Institute for Technical Ceramics, Marie-Curie-Str. 17, D-07629 Hermsdorf, Germany

ST. BARTH*
Friedrich Schiller University, Institute for Inorganic and Analytical Chemistry, August-Bebel-Str. 2, D-07743 Jena, Germany

The hydrolysis of 0.06 mol dm^{-3} $Fe(NO_3)_3$ solutions was followed at 65 °C by means of pH and dynamic light scattering measurements. The hydrolysis products were characterized by transmission electron microscopy and nitrogen adsorption. Depending on the heating procedure different phases were observed, i.e. α-FeOOH (goethite) was formed on heating a 0.06 mol dm^{-3} solution to 65 °C, and α-Fe_2O_3 (hematite) if an appropriate amount of a concentrated stock solution was added to the preheated water at 65 °C. An explanation of this behaviour is offered by taking into account the possible formation of quite different structural units of both solid phases in the course of the hydrolysis process.

1. Introduction

Hydrolysis of iron salt solutions and the resulting products (iron oxides and oxohydroxides) play an important role in mineralogy and soil science, corrosion, biology, and in many industrial applications (pigments, catalysts, ceramics).

Despite numerous studies of the processes involved the mechanisms of the solid phase formation are still not fully understood, due to the tremendous sensibility of the reactions to even minor changes in the experimental conditions.

While the investigation of particle growth processes from ferric chloride solutions has made good progress in recent years [1–4], there are few studies dealing with ferric nitrate solutions. The weak complexing behaviour of the nitrate ion makes it easier to elucidate the effects of other conditions such as iron concentration and temperature on the properties of the hydrolysis products. The large amount of thermodynamic data to characterize the state of the starting solutions at different temperatures, iron(III) concentration and ionic strength was carefully reviewed by Sylva [5] and Flynn [6].

The most systematic approach to describe the hydrolysis processes in ferric nitrate solutions was carried out by Dousma and de Bruyn [7] by go-stop-reverse-stop titrations of acidified 0.0625 mol dm^{-3} solutions with NaOH with simultaneous observation of the changes in optical density. This led to the determination of characteristic pH_A and pH_B values. Above pH_A the solution composition could not be longer described by monomer and dimer complexes only, whereas above pH_B the reverse titration could not be performed reversibly. The latter observation was identified with the onset of the formation of oxo bridges known as oxolation. Aging studies disclosed a phase of primary particles of about 4 nm that formed clusters of 20–50 nm [8] in good agreement with ultracentrifugation experiments of Murphy *et al.* [9].

Using small-angle X-ray scattering Bottero *et al.* [10] determined a size of 0.7–1.35 nm for primary particles formed by the addition of NaOH to 0.01 mol dm^{-3} ferric nitrate solution leading to OH/Fe ratios of 1.5–2.8 in the solutions. The fractal dimension was characteristic for cluster-cluster aggregation of these primary particles.

In all investigations described above the hydrolysis was initiated by the addition of base at room temperature resulting in the formation of α-FeOOH. The controlled base addition avoiding local inhomogeneities, however, is difficult to realize, since local fluctuations of salt concentration and pH at the inlet point can not be

* Author to whom all correspondence should be addressed.

avoided, which seems to be an important intervention in the system under investigation. In contrast, Matijević and Scheiner [11] hydrolyzed ferric nitrate solutions, acidified by HNO_3, at 100 °C and found mostly nearly spherical α-Fe_2O_3 particles at starting concentrations of 0.01–0.04 mol dm^{-3}.

A review of the obtained precipitation products and their phase transformations is given by Blesa and Matijević [12]. A more theoretical approach to explain the hydrolysis of the ferric ion among other metal cations was presented by Henry *et al.* [13], introducing a Partial Charge Model.

Recently, Ocaña *et al.* [3] used the formulation of Matijević and Scheiner [11] to produce ellipsoidal hematite particles in 0.02 mol dm^{-3} ferric nitrate solutions with 0.05 mol dm^{-3} HNO_3 at 100 °C for a more thorough investigation of the growth mechanism. Finding both, goethite and hematite at low aging times, they suggest a three step formation mechanism consisting of goethite precipitation, heterogeneous nucleation of hematite, and hematite growth.

The goal of the study described in this paper was not the precipitation of monodispersed particles of a special morphology, but to provide more information about the mechanisms leading to the formation of goethite or hematite in aqueous $Fe(NO_3)_3$ solutions. The hydrolysis processes were initiated at a temperature of 65 °C without the addition of any precipitating or growth modifying agent, in order to change the reaction conditions as little as possible. Two different methods are used to reach the final temperature. In the first, a 0.06 mol dm^{-3} solution was heated up to 65 °C, while in the second a calculated amount of a stock solution, necessary to generate a final concentration of 0.06 mol dm^{-3}, was added to water that had been preheated to 65 °C.

The processes were followed *in situ* by measuring pH, scattering intensities, and hydrodynamic diameters determined by dynamic light scattering. The reaction products were characterized.

2. Experimental

Stock solutions (2–3 mol dm^{-3} of $Fe(NO_3)_3 \cdot 9H_2O$ p.a., MERCK) did not show any changes during 12 weeks. Their iron content was determined gravimetrically.

2.1. Precipitation procedures

Method 1. The stock solution was diluted with distilled water of room temperature to 0.06 mol dm^{-3} and 11 of the diluted solution in a round flask was placed in an oven at 65 ± 1 °C. The change in solution temperature with time is given in Fig. 1.

Method 2. The appropriate amount of the stock solution was added to distilled water preheated to 65 °C in a 11 round flask to give 11 of 0.06 mol dm^{-3} solution that was further aged in the oven at 65 ± 1 °C.

After given reaction times, the suspensions were filtered as hot as possible by pressure filtration through a 0.22 μm PTFE membrane and dried at room temperature in air. Fe^{3+} concentrations in the filtrate were determined photometrically as the complex with sulfosalicylic acid.

pH measurements could not be carried out in the oven. Instead, they were performed in the same reaction vessel at 65 °C in an oil bath and are, therefore, in Method 1 not directly comparable to the processes in the oven, since the heating to 65 °C was completed in a shorter time.

Light scattering intensities were measured at a scattering angle of 90° with the ELS 800 instrument (Otsuka Electronics) using a 10 mW He-Ne laser (632.8 nm) at 65 °C. A sample was taken from the flask in the oven

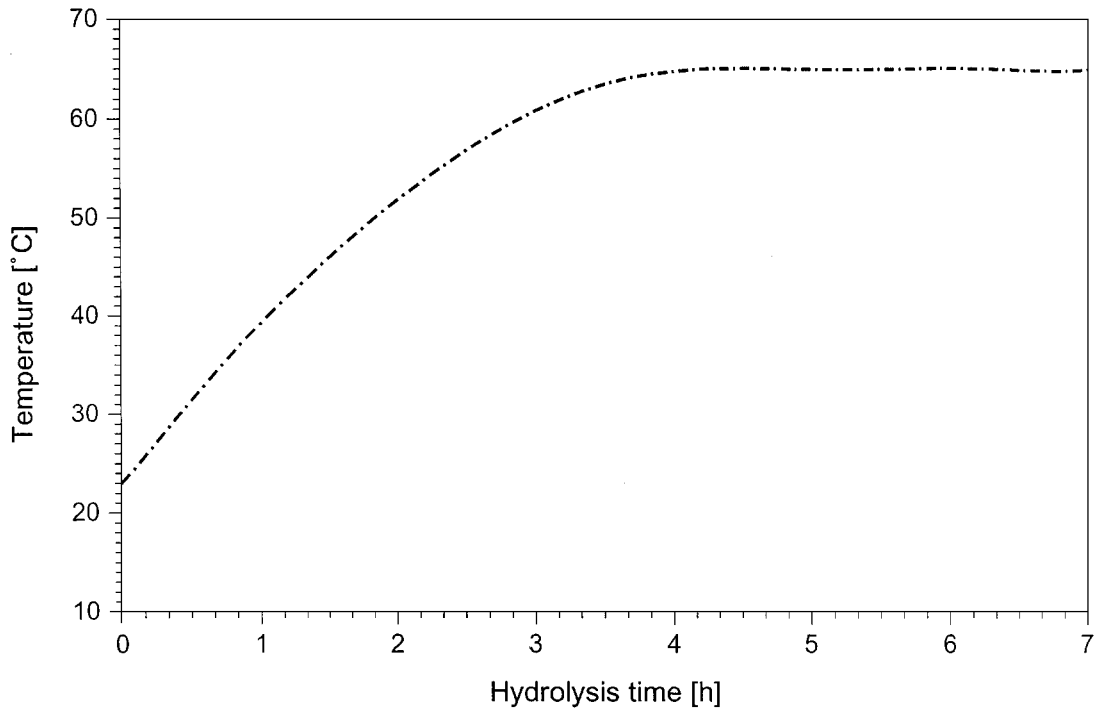

Figure 1 Dependence of the solution temperature on the reaction time, Method 1.

and transferred quickly in a preheated 1 mm quartz cuvette into the sample holder of the instrument at 65 °C. During the first 4 hours in Method 1 the temperature in the sample holder was adjusted to the temperature of the solution in the oven according to Fig. 1.

The hydrodynamic diameters were determined with the same equipment by dynamic light scattering (DLS) measurements from the intensity fluctuations of the scattered light [14] by the *method of cumulants* [15]. The calculated average diameter is a harmonic *z* average [16]; i.e. it is close to the upper boundary of the distribution of particle diameters.

The precipitates were characterized by X-ray diffractometry, transmission electron microscopy (TEM), selected area diffraction (SAD) and sorption measurements (automated sorptometer, Porous Materials Inc.). Specific surface areas were determined by the BET method, and the total pore volumes by the Pierce method [17].

3. Results

3.1. Method 1

In their review Blesa and Matijević [12] proposed a scheme of overlapping deprotonation and olation reactions (Scheme 1).

These processes take place in the systems investigated here as well, followed by oxolation reactions

$$\sim\text{Fe-OH} + \text{HO-Fe}\sim \rightarrow \sim\text{Fe-O-Fe}\sim + \text{H}_2\text{O} \quad (1)$$

because the initial pH (2.1 ± 0.1) at room temperature is in the region of the pH_B (2.0), as determined by Dousma and de Bruyn [8] for 0.0625 mol dm^{-3} $Fe(NO_3)_3$ solutions at 24 °C. According to these authors, above pH_B irreversible processes take place, which are assumed to be oxolation processes.

Due to the need to perform the pH measurements in an oil bath instead of the oven, the heating regime for the samples and during the pH measurements was not exactly the same in this method. In the oil bath the reaction temperature was achieved in a shorter time, so that the pH curve (Fig. 2) should reflect only qualitatively the processes in the solution. The pH was decreased from 2.2 to 2.0 by deprotonation during the first hour. This effect was compensated by a proton consuming process during the second hour until the temperature reached 65 °C. Since neither olation nor oxolation are proton consuming the deprotonation equilibrium seems to be shifted back. After two hours the deprotonation reactions dominated again, and a drop of pH to 1.9 was observed that continued after a solid phase had begun to form.

The scattering intensity during the hydrolysis process (Fig. 3) indicated the formation of nuclei between 4 and 5 h. As soon as the scattering intensity was strong enough to compute hydrodynamic diameters, values of about 100 nm were found. Since a further increase of the scattering intensity was not accompanied by larger particle diameters, the number of particles must have increased. After 13 h sedimentation is observed so that samples are not longer representative of the suspension properties, and the solid content is too high to evaluate DLS data.

Properties of the precipitation products separated from the suspension after given reaction times are listed in Table I. After 24 h more than one half, and after 144 h 2/3 of the initial Fe^{3+} concentration is

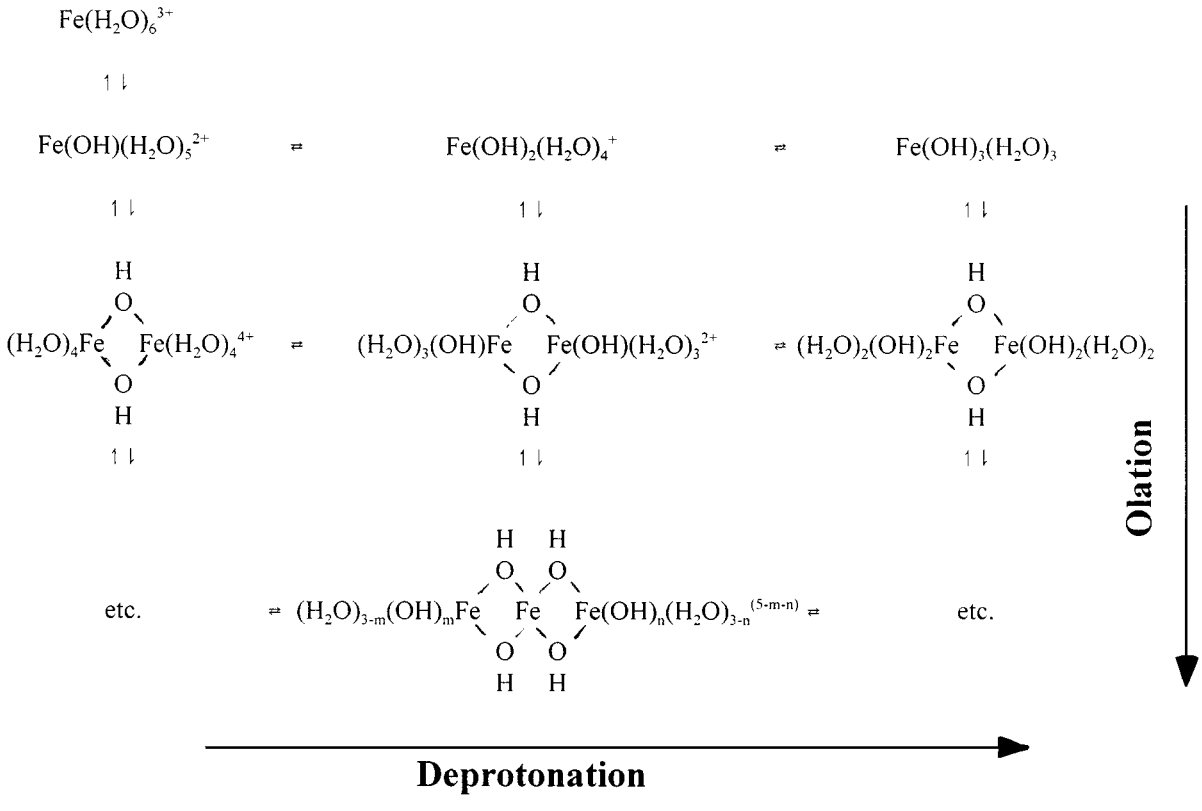

Scheme 1 Olation reaction matrix [12].

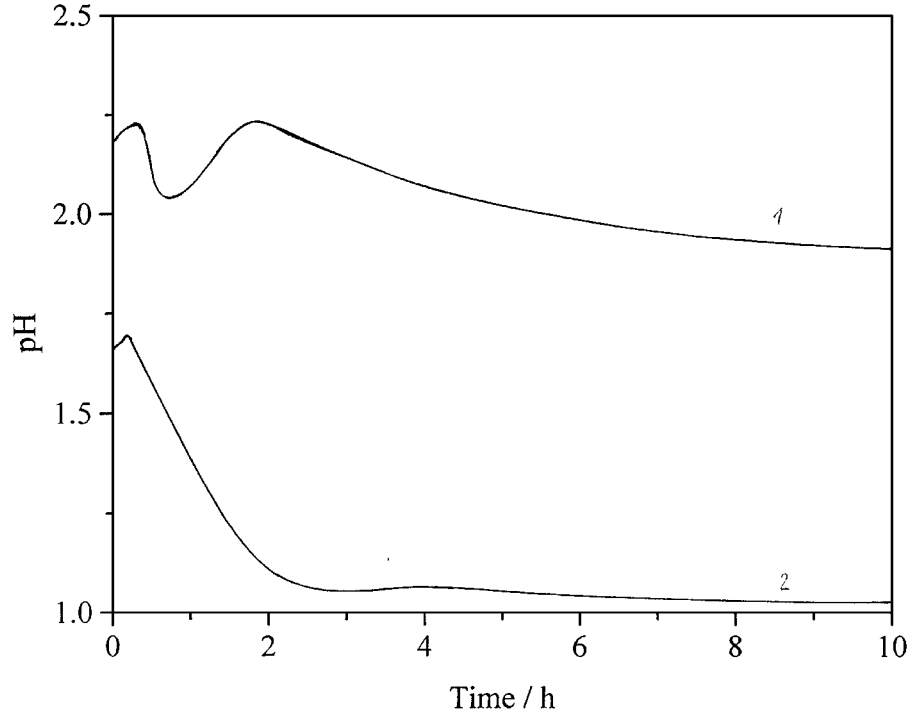

Figure 2 Dependence of the pH on the reaction time in 0.06 mol dm^{-3} $Fe(NO_3)_3$ solutions at 65 °C; (1) Method 1, (2) Method 2, pH_B in 0.0625 mol dm^{-3} $Fe(NO_3)_3$ solutions at 24 °C = 2.0 [8] (see text).

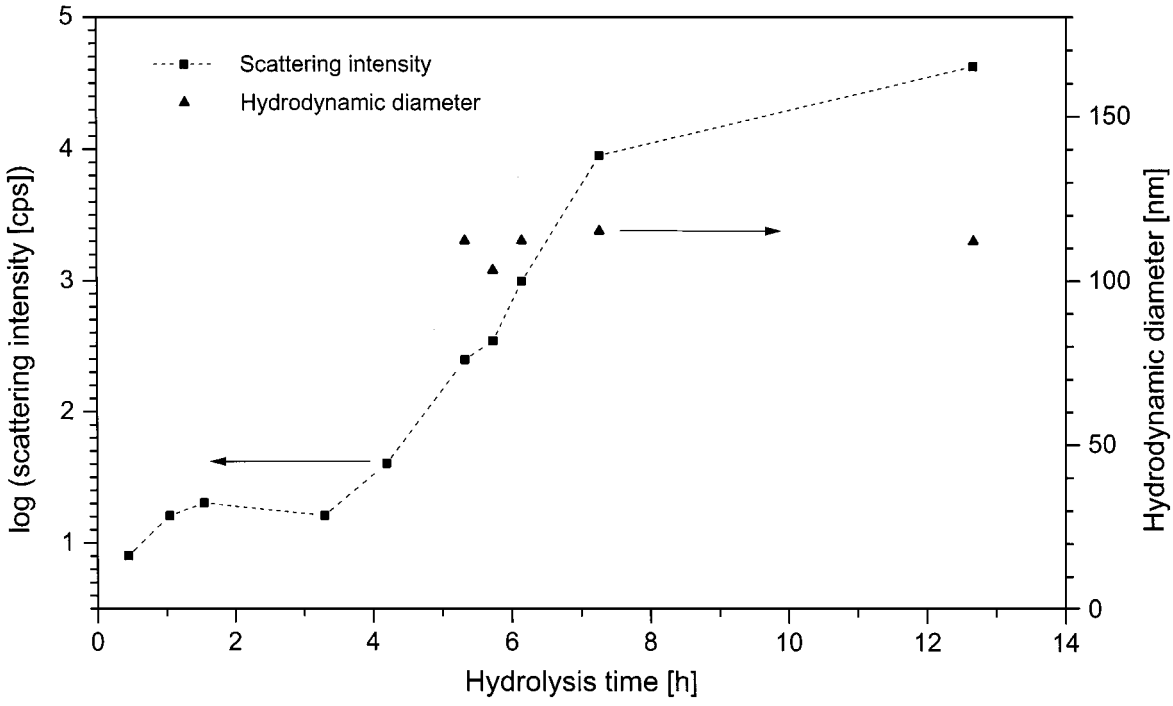

Figure 3 Scattering intensities and hydrodynamic diameters, Method 1.

TABLE I Properties of α-FeOOH powders prepared in 0.06 mol dm^{-3} $Fe(NO_3)_3$ solutions at 65 °C, Method 1

Reaction time (h)	pH_e	$[Fe^{3+}]$ (mol dm^{-3})	BET surface area (m^2 g^{-1})	Total pore volume (cm^3 g^{-1})
12	1.53		112	0.469
24	1.38	0.028	94	0.321
48	1.30		78	0.260
72	1.34		75	0.260
144	1.22	0.020	73	0.134

precipitated in the solid phase. The decreasing pH values of the filtrates show that the precipitation process was not completed during that time. SAD studies indicate the presence of α-FeOOH as the major phase, together with a small amount of α-Fe_2O_3 that is too small to be detected by the X-ray diffraction (Fig. 4). Transmission electron micrographs of a sample reacted for 48 h are shown in Fig. 5, which displays aggregates (diameter 50–125 nm) corresponding to the hydrodynamic diameter. These aggregates consist either of fine

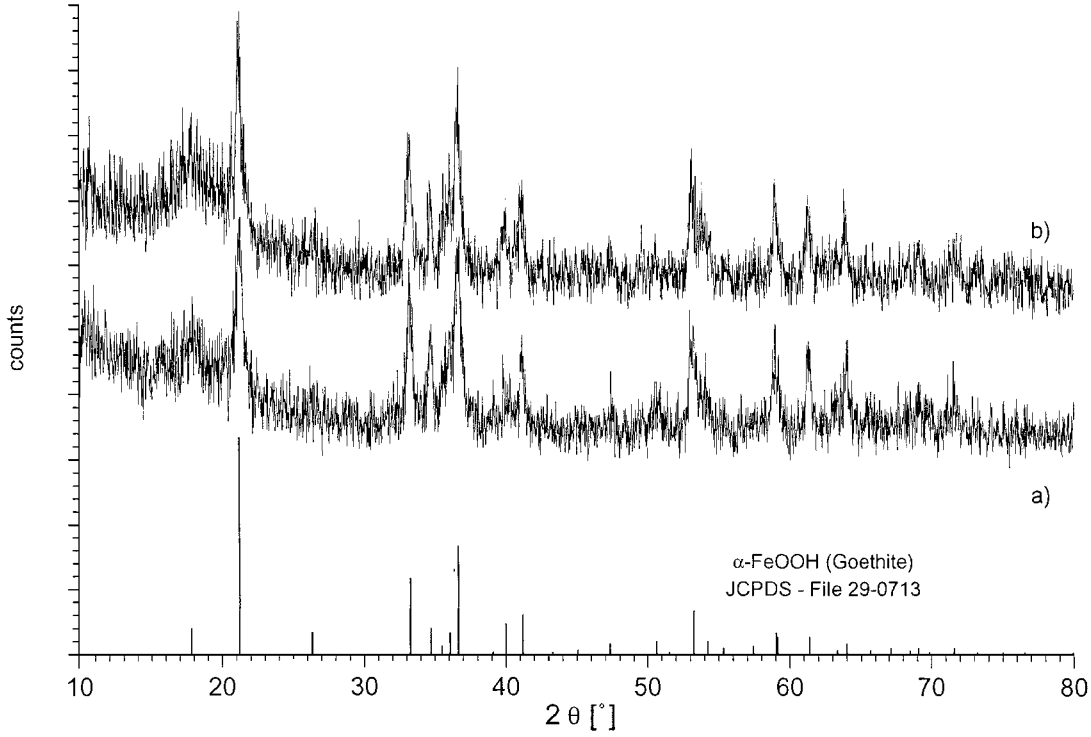

Figure 4 XRD patterns of samples prepared by Method 1 from 0.06 mol dm^{-3} $Fe(NO_3)_3$ at 65 °C, aging times (a) 24 h, (b) 144 h.

needles with a length of about 100 nm or of primary particles (5–10 nm).

BET surface areas are relatively high (70–115 m^2/g). The diameter of dense spherical particles of 11–20 nm calculated from the BET surface area agrees well with the dimension of the observed primary particles.

3.2. Method 2

In contrast to Method 1 the pH of the solution already dropped to ∼1.7 at the beginning of the hydrolysis and decreased further during the following 2 h (Fig. 2). As shown in Fig. 6, the scattering intensity rose above dark current after 1 h and increased slowly during the next 20 h. Initially, hydrodynamic diameters are not larger than 30–50 nm. These particles aggregate due to the salt concentration in the system ($c_{NO_3^-} = 0.18$ mol dm^{-3}) that is above the critical coagulation concentration of 0.1 mol dm^{-3} [11]. These processes yielded species with hydrodynamic diameters of 300–400 nm in the course of the next 20–30 h.

Table II lists properties of the precipitation products separated from suspensions obtained by Method 2 with increasing reaction times. Particles produced at less than 20 h could not be separated by filtration. Instead, one sample was centrifuged after 16 h. This solid had already the α-Fe_2O_3 structure. Transmission electron micrographs of this sample show aggregates that are considerably smaller than those of a sample reacted for 144 h. This fact is also reflected in the respective BET surface areas (140 and 98 m^2/g) shown in Table II. XRD results of the last sample shown in Fig. 7 prove the α-Fe_2O_3 structure while electron micrographs (Fig. 8) show aggregates with diameters between 20 and 80 nm made up of primary particles with diameters ≤10 nm. There are few needles with a thickness below 10 nm. The *d* values calculated from the radii of the rings of the SAD pattern (Fig. 8a) agree well with those known for hematite from the JCPDS Diffraction Data Files [18]. The aggregates are shown to consist of small single crystals of hematite (Fig. 8b). The needles show lattice planes (arrow in Fig. 8c), i.e. they are crystalline, the spacing of these planes can be attributed to those of goethite. After very long times (608 h) the reaction was nearly completed. The large BET specific surface areas (Table II) can be explained by the small diameter of the primary particles. Their size determined from the BET data (8–11 nm diameter) are in good agreement with the diameters found by TEM.

TABLE II Properties of α-Fe_2O_3 powders prepared in 0.06 mol dm^{-3} $Fe(NO_3)_3$ solutions at 65 °C, Method 2

Reaction time (h)	pH_e	$[Fe^{3+}]$ (mol dm^{-3})	BET surface area (m^2 g^{-1})	Total pore volume (cm^3 g^{-1})
16			140	0.315
24	1.29	0.027	132	0.213
48			105	0.315
72			119	0.186
144			98	0.229
608	1.02	0.008	81	0.218

4. Discussion

It is surprising that the hydrolysis of 0.06 mol dm^{-3} $Fe(NO_3)_3$ solution yields two different products, namely α-FeOOH (Method 1) and α-Fe_2O_3 (Method 2) under nearly identical conditions except the heating regime up to 65 °C, which seems to be very important.

To explain this behaviour, it is useful to inspect the structures of α-FeOOH and α-Fe_2O_3 (Fig. 9). The

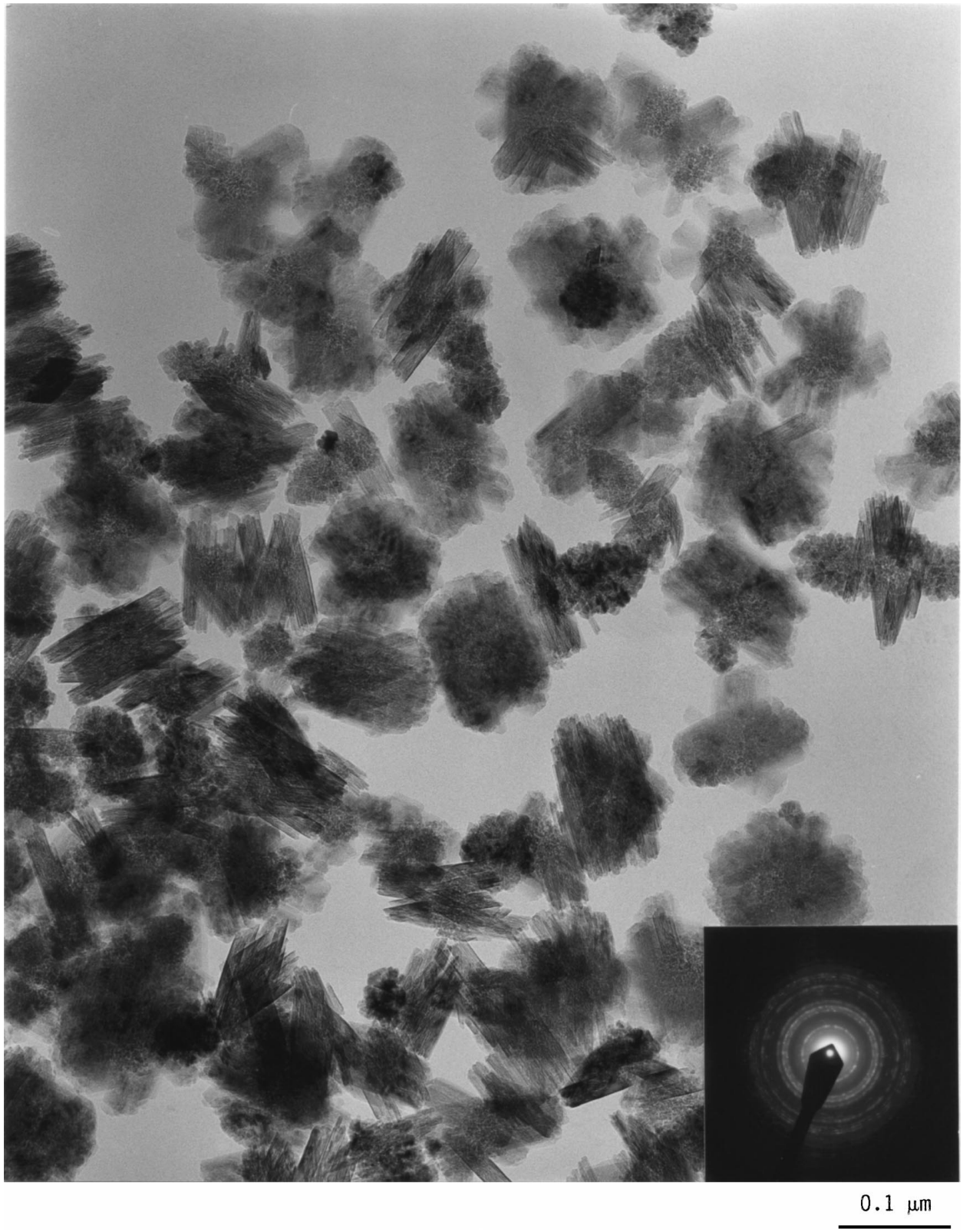

Figure 5 TEM and SAD of a sample prepared by Method 1 from 0.06 mol dm^{-3} $Fe(NO_3)_3$ at 65 °C, aging time 48 h.

structural units of goethite consist of double octahedra built up by **edge**-sharing of two $Fe(O;OH)_6$ octahedra. These units are further connected by **corner**-sharing to a three-dimensional network.

Due to the different Fe : O ratio (1 : 1.5) hematite has a higher degree of condensation within the three-dimensional network than α-FeOOH (Fe : O = 1 : 2), which is phenomenologically expressed by a significant higher density of hematite ($\rho = 5.26$ g cm^{-3}) compared with goethite ($\rho = 4.26$ g cm^{-3}). This higher density is the consequence of the existence of **face**-shared FeO_6 octahedra linked by edge-sharing. A second criterion for the higher degree of network condensation in hematite is the estimated molar volume related to a mole of oxygen ions giving 10.43 cm^3 mol^{-1} for goethite and 10.10 cm^3 mol^{-1} for hematite despite of a

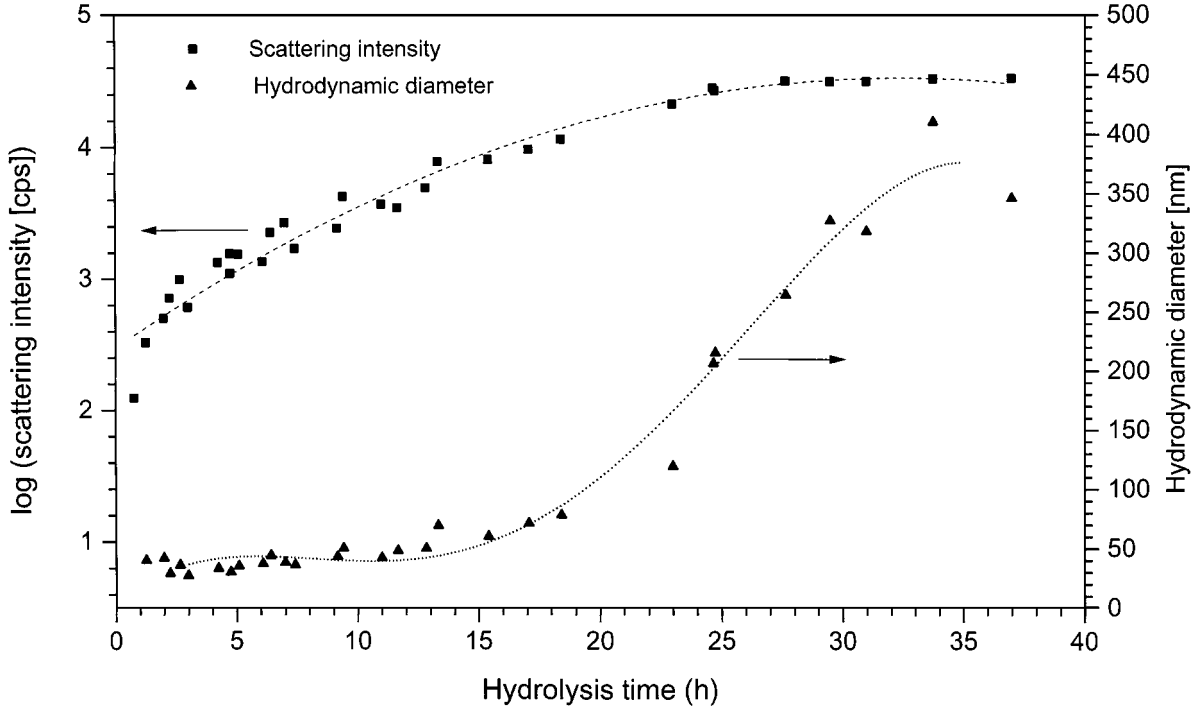

Figure 6 Scattering intensities and hydrodynamic diameters in 0.06 mol dm^{-3} $Fe(NO_3)_3$ solutions at 65 °C, Method 2.

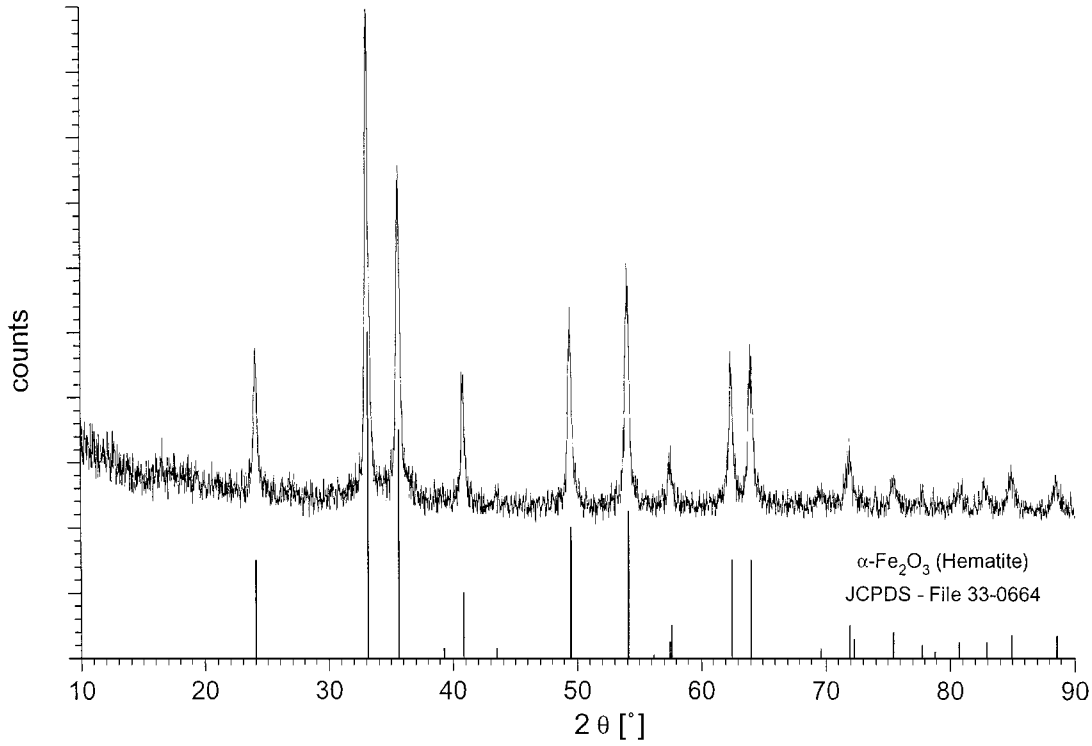

Figure 7 XRD patterns of a sample prepared by Method 2 from 0.06 mol dm^{-3} $Fe(NO_3)_3$ at 65 °C, aging time 144 h.

higher Fe^{3+} content (0.667 per oxygen ion) in α-Fe_2O_3 than in α-FeOOH (0.5 per oxygen ion, Table III).

Since in our study α-FeOOH and α-Fe_2O_3 have been formed without further thermal treatment of the solid products the described structural units of these solid phases must have been formed during the hydrolysis of the iron(III) nitrate solution. Considering the quite complex scheme of deprotonation and olation (Scheme 1) and the oxolation reaction (Equation 1) during the hydrolysis regarding the described structural units it is easily seen that the edge-sharing double-octahedra $[(H_2O;OH)_4Fe(O;OH)_2Fe(H_2O;OH)_4]^{n+}$ can be expressed in terms of the first stage of the beginning structure formation. Together with the degree of deprotonation and hence with their net charge, the life-time of these species is obviously responsible for the proceeding linkage of the double-octahedra to a network structure.

In Method 2 the high temperature from the very beginning of the hydrolysis causes a steep pH drop, i.e. a shift of the deprotonation and polymerization reactions towards the deprotonated and the polymeric species.

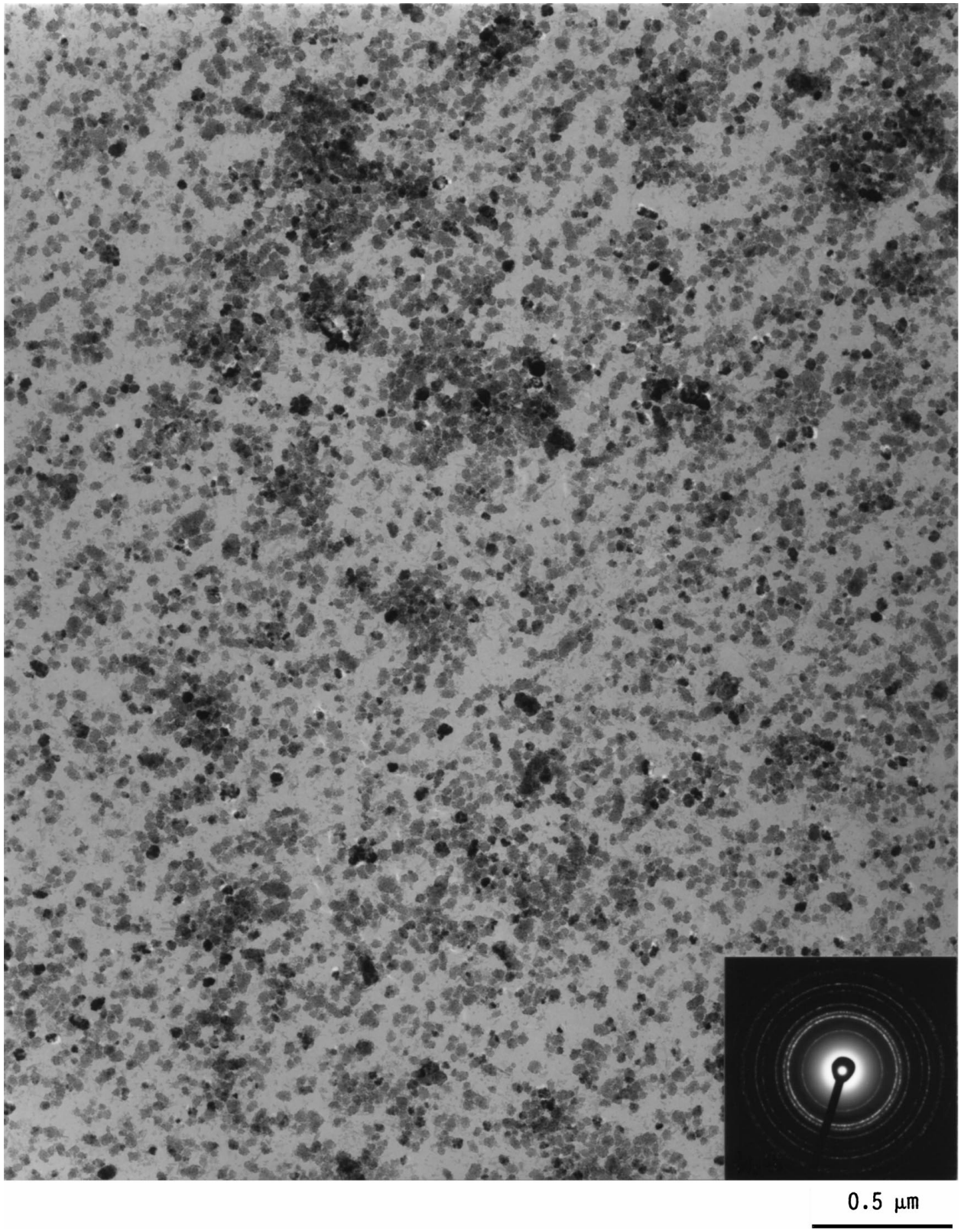

Figure 8 TEM and SAD of a sample prepared by Method 2 from 0.06 mol dm^{-3} $Fe(NO_3)_3$ at 65 °C, aging time 144 h.

Rate constants [12] show that reactions involving water displacement become faster as the charge per iron atom decreases. Essential processes take place at pH ≈ 1.1–1.2 (in contrast to 1.7–1.8 in Method 1). Dimers ("double-octahedra") and oligomers are quickly polymerized, thus, their availability becomes lower. After about 75 min the polymeric network must have a size of several nanometers, since the scattering intensity is large enough to compute hydrodynamic diameters. At the same time the production of deprotonated monomers and dimers has almost stopped—the pH remains nearly constant after 2 h. In other words, the "nucleation" process has finished. Instead, an "intramolecular" condensation of edge-shared octahedra may be favoured leading to the face-sharing of $Fe(O;OH)_6$ octahedra that is necessary for the structural motif of

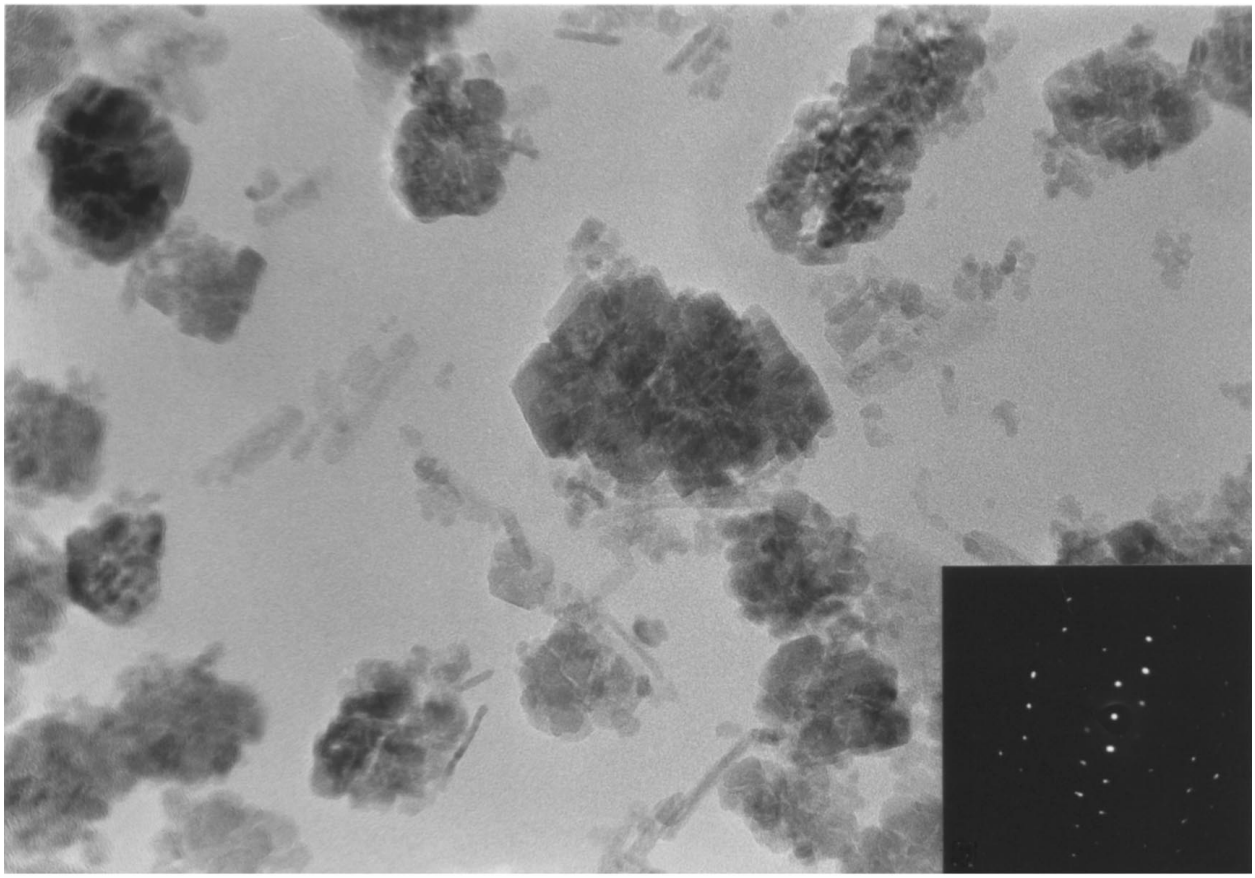

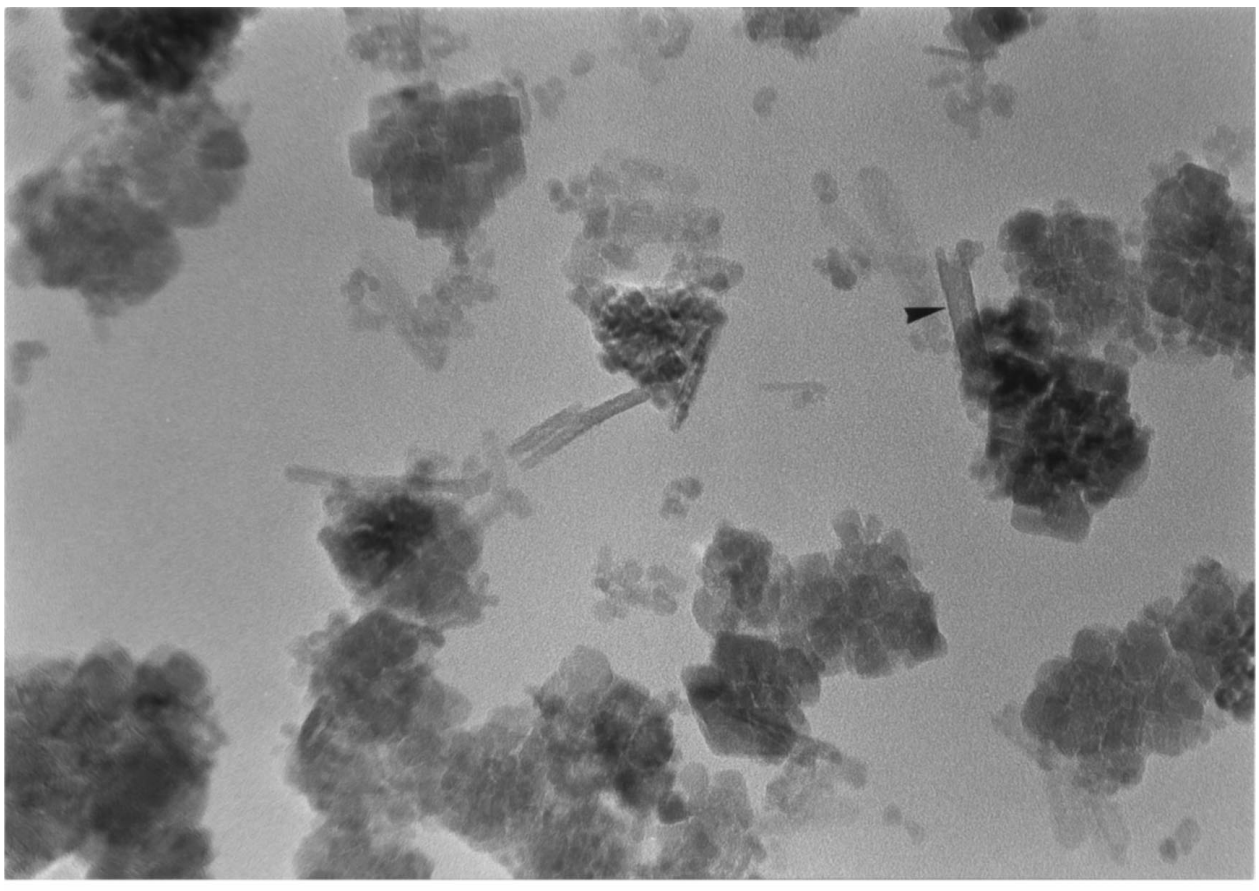

Figure 8 (*Continued*).

hematite, e.g.:

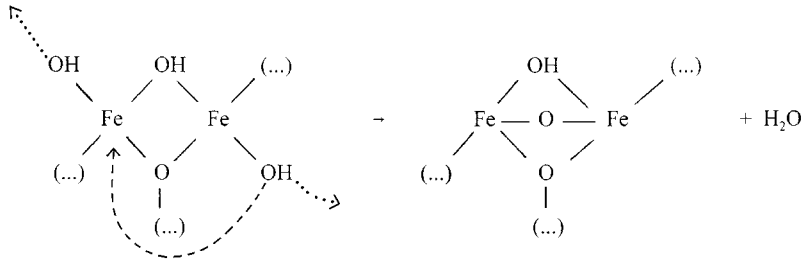

(2)

Since the formation of oligomers has stopped, particle growth proceeds by direct deposition of monomers. Thus, the low pH has led to a better separation of particle nucleation and growth causing a relatively monodiperse product (Fig. 8a).

In [3] it is suggested that goethite was precipitated first under similar conditions. The authors used ferric nitrate solutions of a somewhat lower concentration (0.02 instead of 0.06 mol dm^{-3}) and a higher hydrolysis temperature (100 instead od 65 °C). Low solution pH was adjusted by the acidification with HNO_3. The presence of a very small amount of relatively well crystallized goethite needles in our sample (Fig. 8c) formed with Method 2 as long as 144 h (6d) show that some α-FeOOH nuclei must have formed at the beginning as well, although they could not be detected by XRD. It can not be excluded that the initially formed polymer network built both the α-Fe_2O_3 and α-FeOOH structures, where the easier soluble α-FeOOH was mostly dissolved and recrystallized to α-Fe_2O_3.

TABLE III Crystal data for goethite and hematite

	α-FeOOH	α-Fe_2O_3
Crystal system	Orthorhombic	Trigonal
Cell dimensions (Å)	$a_0 = 4.608$	$a_0 = 5.034$
	$b_0 = 9.956$	$c_0 = 13.752$
	$c_0 = 3.0215$	
Formula units per unit cell	4	6
Density (g cm^{-3})	4.26	5.26
Molar weight (g mol^{-1})	88.853	159.692
Volume per unit cell VUC ($Å^3$)	138.618	301.803
VUC · N_L (cm^3 mol^{-1})	83.48	181.75
Molar volume per formula unit (cm^3 mol^{-1})	20.87	30.29
Molar volume per mole Fe^{3+} (cm^3 mol^{-1})	20.87	15.15
Molar volume per mole O^{2-} (cm^3 mol^{-1})	10.43	10.10

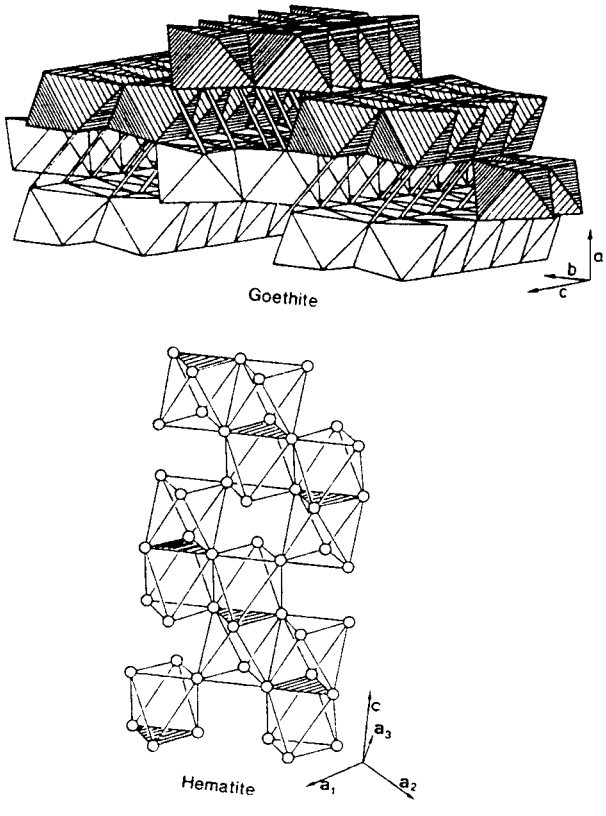

Figure 9 Idealized structures of goethite (a) and hematite (b) [19].

In contrast, at higher pH and slowly increasing temperatures (Method 1) deprotonation and olation reactions lead to the continued formation of dimers and their linkage via edges to the double-octahedra chains in the goethite structure as described in [13]. In this case, nucleation and growth are not separated, causing a large variety of particle shapes and sizes (Fig. 5). The initially formed α-FeOOH structure slowly transforms into α-Fe_2O_3, probably by a dissolution-recrystallization process. The formation of intramolecular bridges as shown in Equation 2 is not very likely.

Interestingly, it also seems to be possible to apply the described formation concept to weathered products of iron(III) minerals in nature provided that the influence of anions such as chloride and sulfate is negligible. The yellow-brown goethite is found in nearly all soils and rocks whereas the red hematite colors especially the soils of tropic and subtropic regions. Higher temperatures and lower water amounts in the latter regions are responsible for this phenomenon [19].

Acknowledgment

Financial support by the BASF AG, Ludwigshafen, is gratefully acknowledged. We wish to thank Dr. E. Schwab and Dr. P. Poganiuch (BASF AG) for helpful discussions and Dr. S. Kohl (BASF AG) for TEM and SAD.

References

1. M. P. MORALES, T. GONZALEZ-CARREÑO and C. J. SERNA, *J. Mater. Res.* **7** (1992) 2538.

2. J. K. BAILEY, C. J. BRINKER and M. L. MECARTNEY, *J. Colloid Interface Sci.* **157** (1993) 1.
3. M. OCAÑA, M. P. MORALES and C. J. SERNA, *ibid.* **171** (1995) 85.
4. T. SUGIMOTO and A. MURAMATSU, *ibid.* **184** (1996) 626.
5. R. N. SYLVA, *Rev. Pure Appl. Chem.* **22** (1972) 115.
6. C. M. FLYNN, *Chem. Rev.* **84** (1984) 31.
7. J. DOUSMA and P. L. DE BRUYN, *J. Colloid Interface Sci.* **56** (1976) 527.
8. *Idem., ibid.* **64** (1978) 154.
9. P. J. MURPHY, A. M. POSNER and J. P. QUIRK, *ibid.* **56** (1975) 270.
10. J.-Y. BOTTERO, D. TCHOUBAR, M. ARNAUD and P. QUIENNE, *Langmuir* **7** (1991) 1365.
11. E. MATIJEVIĆ and P. SCHEINER, *J. Colloid Interface Sci.* **63** (1978) 509.
12. M. A. BLESA and E. MATIJEVIĆ, *Adv. Colloid Interface Sci.* **29** (1989) 173.
13. M. HENRY, J. P. JOLIVET and J. LIVAGE, *Structure Bonding* **77** (1992) 153.
14. N. DE JAEGER, H. DEMEYERE, R. FINSY, R. SNEYERS, J. VANDERDEELEN, P. VAN DER MEEREN and M. VAN LAETHEM, *Part. Part. Syst. Charact.* **8** (1991) 179.
15. D. E. KOPPEL, *J. Chem. Phys.* **57** (1972) 4814.
16. R. FINSY and N. DE JAEGER, *Part. Part. Syst. Charact.* **8** (1991) 187.
17. C. PIERCE, *J. Phys. Chem.* **57** (1953) 149.
18. Joint Committee on Powder Diffraction Standards, JCPDS International Center for Diffraction Data, Pennsylvania, 1993.
19. U. SCHWERTMANN and R. M. CORNELL, "Iron Oxides in the Laboratory" (Verlag Chemie, Weinheim, 1991).

Received 4 September 1997
and accepted 9 November 1998